THE JOURNAL OF PHYSICAL CHEMISTRY B

Article

pubs.acs.org/JPCB

Comparison Studies on Sub-Nanometer-Sized Ion Clusters in Aqueous Solutions: Vibrational Energy Transfers, MD Simulations, and Neutron Scattering

Yuneng Shen,[†,§,¶] Tianmin Wu,[∥,¶] Bo Jiang,[†,¶] Ganghua Deng,[†] Jiebo Li,[‡] Hailong Chen,[‡] Xunmin Guo,[‡] Chuanqi Ge,[†,⊥] Yajing Chen,[†] Jieya Hong,[†] Xueming Yang,[†] Kaijun Yuan,*[,†] Wei Zhuang,*[,†] and Junrong Zheng*[,‡]

[†]State Key Laboratory of Molecular Reaction Dynamics, Dalian Institute of the Chemical Physics, Chinese Academy of Sciences, Dalian, 116023 Liaoning, China

[‡]Department of Chemistry, Rice University, Houston, Texas 77005, United States

[§]University of the Chinese Academy of Sciences, Beijing 100049, China

[∥]Department of Chemical Physics, University of Science and Technology of China, Hefei 230026, China

[⊥]School of Physics and Electronic Technology, Liaoning Normal University, Dalian 116029, China

Supporting Information

ABSTRACT: In this work, MD simulations with two different force fields, vibrational energy relaxation and resonant energy transfer experiments, and neutron scattering data are used to investigate ion pairing and clustering in a series of GdmSCN aqueous solutions. The MD simulations reproduce the major features of neutron scattering experimental data very well. Although no information about ion pairing or clustering can be obtained from the neutron scattering data, MD calculations clearly demonstrate that substantial amounts of ion pairs and small ion clusters (subnanometers to a few nanometers) do exist in the solutions of concentrations 0.5 M*, 3 M*, and 5 M* (M* denotes mole of GdmSCN per 55.55 mole of water). Vibrational relaxation experiments suggest that significant amounts of ion pairs form in the solutions. Experiments measuring the resonant energy transfers among the thiocyanate anions in the solutions suggest that the ions form clusters and in the clusters the average anion distance is 5.6 Å (5.4 Å) in the 3 M* (5 M*) $Gdm_{-D}SCN/D_2O$ solution.

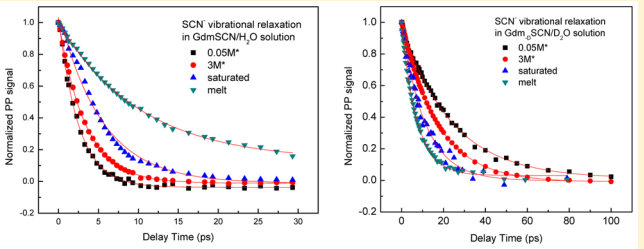

1. INTRODUCTION

Ion pairing and clustering in aqueous solutions are among the most fundamental chemical phenomena in nature. They play important roles in determining the properties of aqueous solutions, for example, activities, vapor pressures, osmotic pressures, and the kinetics of crystal growth. For example, the classical nucleation theory assumes that the bulk energy of a nascent nucleus drives nucleation, where its structure is that of the macroscopic bulk material. The formation of the nucleus occurs through stochastic fluctuations on microscopic length scales. In consequence, classical precritical nuclei are rare species, and the underlying cluster size distribution has an average size of molecular monomers or dimers.[1−6] Recent advances in biomineralization suggest a possible alternative aggregation-based pathway that cannot be reconciled with the notion of classical nucleation theory: when ions meet in solution based on stochastic collisions, they form stable prenucleation clusters the structures of which might not relate to the crystal. The nucleated clusters subsequently crystallize to generate the final stable crystal.[1−6] One way to verify and study this possible nucleation mechanism is to directly determine the structures of these prenucleation clusters.

Analytical ultracentrifugation, which detects species in solution according to the difference in their sedimentation coefficients, can confirm the existence of clusters in solutions.[1,2,7] However, it is not an in situ method, and it cannot separate those transient subnanometer clusters.

Neutron-scattering method is a powerful technique for studying solution structures. Combined with isotope labels, the method can be used to obtain information about the anion and cation hydration structures,[8] such as revealing the water structuring around simple monatomic ions,[9−11] noble gases,[12,13] and tetramethylammonium with quasi-spherical symmetry.[14,15] In addition, the method can also probe strong ion pairing effects, which result in large (greater than tens of nanometers) ion aggregations in aqueous electrolyte solutions. For example, by comparing the experimental heavy atom

Received: May 11, 2015
Revised: June 23, 2015
Published: July 2, 2015

DOI: 10.1021/acs.jpcb.5b04530
J. Phys. Chem. B 2015, 119, 9893−9904

correlation function of Gdm_2SO_4 aqueous solution with that of GdmSCN aqueous solution, it was found that the hydration of the Gdm^+ ion in Gdm_2SO_4 aqueous solution deviates significantly from that of the GdmSCN aqueous solution in which the ions are much more homogeneously distributed. The experimental results are consistent with the MD simulation results that in the Gdm_2SO_4 aqueous solution the ions aggregate into mesoscopic clusters but no such large aggregations exist in the GdmSCN solution.[16]

The neutron scattering results on the Gdm_2SO_4 and GdmSCN aqueous solutions[16] were somehow misunderstood by many people as the evidence to prove that no ion pairing or clustering exists in the 3 M GdmSCN aqueous solution. (We frequently encountered questions arising from such a misunderstanding, when presenting our ion clustering results concluded from the vibrational energy transfer measurements.) In fact, the neutron scattering method is insensitive to weak ion pairing or subnanometer scale clustering. For example, in the 3 M GdmSCN aqueous solution, the MD simulations show that guanidinium−thiocyanate pairs tend to randomly distribute throughout the solution.[16] However, the hydration structure of the Gdm^+ ions in GdmSCN aqueous solution in which ions form weak ion pairing cannot be experimentally distinguished from that without ion pairing. Meanwhile, although the measured scattering is a direct function of the structure of the solution, which is undoubtedly crucial information, it cannot answer the question whether Gdm^+ and SCN^- form clusters in water. Six pairs of distribution functions (g_{CC}, g_{SS}, g_{CN}, g_{CS}, g_{NS}, and g_{SO}) are neglected in processing the neutron scattering data, as together they contribute less than 10% to the total distribution function ${}^nG_Y^Y$s.[16] (The detailed derivation of pair distribution functions of GdmSCN solution is provided in Supporting Information.) As a result, what one obtains from the experiments is

$$ {}^nG_Y^Y \approx 0.44502g_{OO} + 0.31069g_{NO} + 0.11025g_{CO} + 0.05424g_{NN} - 1 \quad (1) $$

where g_{OO}, g_{NO}, g_{CO}, and g_{NN} are pair functions of O−O, N−O, C−O, and N−N atom pairs. The contribution of g_{NN}, which can confirm heteroion pairing, is very small (<6%). Experimental results show that g_{NN} overlaps with g_{OO}, g_{NO}, and g_{CO}, and its intensity is overwhelmed.[16] In other words, the contribution of ion−ion pair correlations to the total scattering pattern is too small compared with the contributions from water−water and water−ion interactions.

Dynamic light scattering is another technique for directly detecting cluster populations in solution. But the size of clusters that it can resolve is submicrometer scale or larger.[17] Subnanometer scale ion aggregations like those in the GdmSCN aqueous solution revealed by MD simulations are very challenging to detect by the dynamic light scattering method.

Raman spectroscopy is a powerful method to probe ion clustering as well, albeit many assumptions are required to interpret the results. For example, Raman experiments suggested the presence of clusters in electrolyte ($NaNO_3$,[18,19] KH_2PO_4, and $(NH_4)H_2PO_4$[20]) aqueous solutions. In these studies, the concentration-dependent peak absorption line shapes were recorded. On the basis of the analyses of the line shapes, it was concluded that the evidence of ion clustering was obtained. However, many molecular parameters can affect vibrational absorption line shapes. It is not immediately clear how the contribution of ion pairing and clustering can be separated from other contributions, for example, the structural changes of hydration shells.[21]

In summary, the neutron and dynamic light scattering and the Raman spectroscopy methods are capable of detecting large ion clusters of submicrometer size. For smaller clusters, it is very challenging for the scattering techniques. Recently, we demonstrated that some of these small ion clusters can be directly measured with the intermolecular vibrational energy transfer methods, which can directly determine the ion−ion distances.[22−27]

In this work, by comparing the results from MD simulations, vibrational energy transfer and relaxation measurements, and neutron scattering data, we demonstrate that ion clusters that are too small for neutron scattering technique to detect can be studied with the ultrafast nonlinear vibrational spectroscopic methods.

2. METHODS

2.1. Experimental Methods. The experimental setup has been described elsewhere.[28−31] Briefly, the output of one oscillator is divided into two beams entering a picosecond amplifier and a femtosecond amplifier. The picosecond amplifier (~2.8 mJ/pulse) pumps an optical parametric amplifier (OPA) and noncollinear difference frequency generator (NDFG) system to produce ~1.4 ps (vary from 1.0−1.5 ps in different frequencies) mid-IR pulses with a bandwidth ~15 cm^{-1} in a tunable frequency range from 500 to 4000 cm^{-1} with energy 1−40 μJ/pulse at 1 kHz.The femtosecond amplifier (2.8 mJ/pulse) pumps another OPA and NDFG system to produce ~140 fs mid-IR pulses with a bandwidth ~200 cm^{-1} in a tunable frequency range from 500 to 4000 cm^{-1} with energy 1−40 μJ/pulse at 1 kHz. In the nonlinear experiments, the picosecond IR pulse is the excitation beam (the excitation power is adjusted based on need). The femtosecond IR pulse is the probe beam which is frequency resolved by a spectrograph yielding the ω_3 axis of a 2D spectrum. Scanning the pump frequency yields the ω_1 axis of the spectrum. Two polarizers are inserted into the probe beam pathway (one of them is located immediately behind the sample) to selectively measure the parallel or perpendicular polarized signal relative to the pump beam. The entire system is computer controlled. Vibrational lifetimes are obtained from the rotation-free signal $P_{life} = P_{\parallel} + 2P_{\perp}$, where $P_{\parallel}$ and $P_{\perp}$ are parallel and perpendicular data, respectively. Rotational relaxation times are acquired from $R = (P_{\parallel} - P_{\perp})/(P_{\parallel} + 2P_{\perp})$.

Guanidinium thiocynate was purchased from Aladdin. The deuterated NH (ND) of the guanidinium thiocynate was prepared by deuterium exchange with methanol-OD.To obtain the deuterated guanidinium thiocynate, 1 g of undeuterated guanidinium thiocynate was dissolved in 10 g of methanol-OD and stirred for 0.5 h. The solvent was then removed under vacuum. The procedure was repeated three times, and compounds with >90% deuteration of the NH were obtained.

D_2O was purchased from C/D/N Isotopes Inc. KSCN and $KS^{13}C^{15}N$ were purchased from Aldrich and used as received. The liquid samples, used for the experimental measurements, were contained in a sample cell composed of two CaF_2 windows separated by a Teflon spacer. The thickness of the spacer was adjusted accordingly to the optical densities. Experiments were performed at 23 and 130 °C.

Solutions contain 0.05, 0.5, 3, and 5 mol of GdmSCN per 55.55 mol of water (hereafter referred to as 0.05, 0.5, 3, and 5

DOI: 10.1021/acs.jpcb.5b04530
J. Phys. Chem. B 2015, 119, 9893−9904

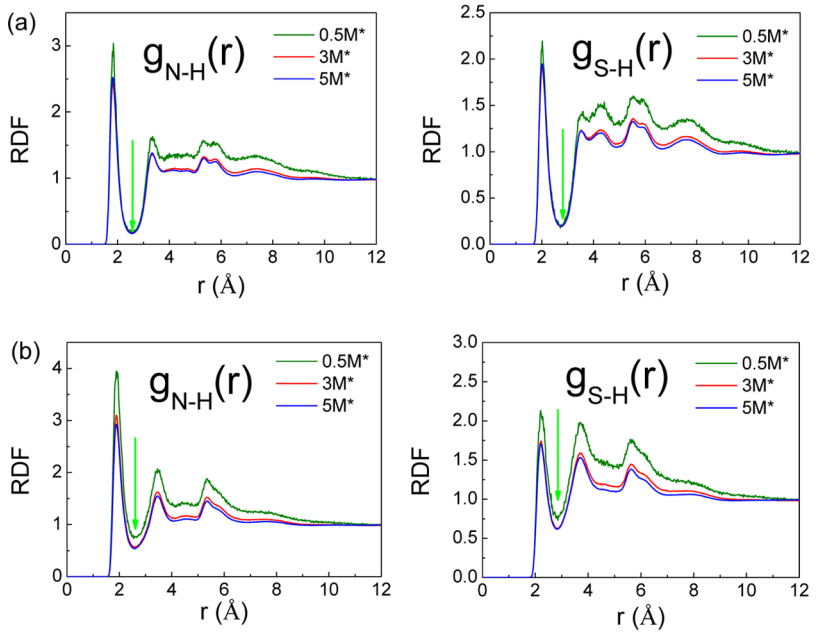

Figure 1. The RDFs of N(SCN$^-$)−H(Gdm$^+$) and S(SCN)−H(Gdm$^+$) for (a) OPLS-AA force field and (b) CHARMM force field. Both of them are calculated in the concentrations of 0.5 M* (olive), 3 M* (red), and 5 M* (blue), respectively. The green arrow shows the first minimum in the radial distribution function.

M* GdmSCN) in H_2O and D_2O (GdmSCN is deuterated). These solutions were prepared by direct dissolution of the salts in water. In our experiment, 2% of KS^{13}C^{15}N is added to the GdmSCN. The $^{13}C^{15}N$ stretching vibration leads to a strong absorption around 1990 cm^{-1}, and the orientational dynamics of these molecules can be conveniently monitored using pump−probe spectroscopy.

The structural and vibrational calculations were carried out as implemented in the Gaussian 09 program suite. The level and basis set used were Becke's three-parameter hybrid functional combined with the Lee−Yang−Parr correction functional, abbreviated as B3LYP, and 6-311+G(d,p).

2.2. Molecular Dynamics Simulation Method. Molecular dynamics simulations were carried out for the GdmSCN aqueous solutions at three different concentrations 0.5, 3.0, and 5.0 mol/kg. The ions were randomly placed and oriented in a cubic box and then solvated by explicit water molecules. All simulations were performed using the program GROMACS 4.6 software package.[32] For 0.5 M* solution, there are 8 SCN$^-$, 8 Gdm$^+$, and 889 water molecules in solution, making aqueous solutions neutral. Furthermore, for 3 M* solution, there are 48 SCN$^-$, 48 Gdm$^+$, and 889 water molecules in solution, making aqueous solutions neutral. For 5 M* solution, there are also 889 water molecules, but 79 SCN$^-$ and 79 Gdm$^+$ in solution. In order to ensure the correctness of our simulations, a different force field for Gdm$^+$ and SCN$^-$ was used to simulate in this work. (1) The OPLS-AA force field[33,34] was used to describe interatomic interactions for Gdm$^+$ and SCN$^-$, and the SPC/E explicit model[35] was used for water because it is compatible with Jorgensen's OPLS-AA force field. (2) As in Mason's work,[16,36] we employed a potential energy function based on the parameters for arginine in the CHARMM27 all-atom force field,[37] with the atomic partial charges assigned symmetrically (atom charges, C 0.64; N −0.80; H 0.46), while the parameters for SCN$^-$ were not modeled using literature potentials as demonstrated in Mason's work[16,36] but literature potentials developed by Vincze et al.,[38] because they have been well tested. The reason to make such a choice is that such potentials developed by Sansone et al.[39] just pay attention to the interaction between thiocyanate and water molecules but do not consider the important interaction parameters between Gdm$^+$ and SCN$^-$ in our simulation system. Although the force field parameters used were not the same in these works, the molecular dynamics simulation set was similar. All bond lengths were constrained using the LINCS (linear constraint solver) algorithm.[40] The system was propagated using the leapfrog algorithm[41] with a time step of 2 fs. The long-range electrostatic interactions were handled by a particle-mesh Ewald algorithm[40,42] with a Coulomb cutoff radius of 12 Å, while the short-ranged van der Waals interactions were truncated using a cutoff of 10 Å. The cubical periodic boundary boxes were employed in molecular dynamic simulation to avoid problems with boundary effects caused by finite size, which has been dimensioned to reproduce the experimental density at ambient conditions. Minimum image conditions[43] were used in these cubical periodic systems. In the simulation, an initial 10 ns NPT ensemble equilibration was carried out. The weakly coupling Berendsen thermostats[44] were employed to keep the system temperature at 300 K with the relaxation time of 0.1 ps. The system pressure was controlled by the weak coupling Berendsen schemes[44] with a coupling time constant of 1 ps. After initial equilibration runs, the production runs were carried out for a 20 ns NVE ensemble equilibrium molecular dynamic simulation with a standard time step of 2 fs to calculate the dynamic properties. The simulation trajectories were saved every 100 steps for the later calculations.

The following criteria was using to define an ion cluster:[45] (1) if the distance between an anion and a cation is less than the distance r for the first minimum in the radial distribution function, we consider that they are "connected"; (2) each ion can reach the other one in the ion cluster through the bridge comprising these kinds of connections. The ion cluster size also can be defined by the total number of ions in one ion cluster, n.

DOI: 10.1021/acs.jpcb.5b04530
J. Phys. Chem. B 2015, 119, 9893−9904

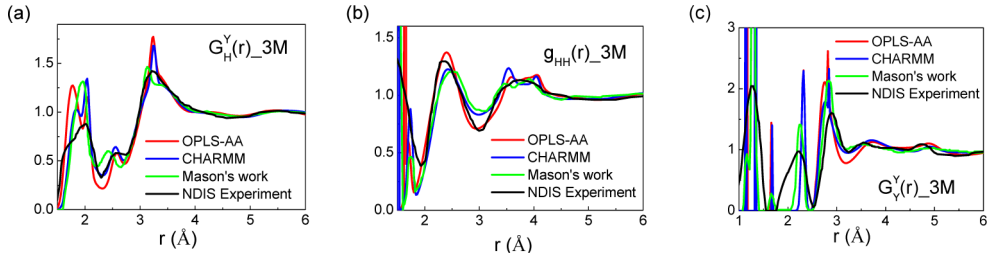

Figure 2. For each radial distribution function for 3 M* GdmSCN solution, (a) $G^{Y}_{H}(r)$, (b) $g_{HH}(r)$, (c) $G^{Y}_{Y}(r)$. The curves of "Mason's work" and "NDIS Experiment" are plotted based on data extracted from published results.[16]

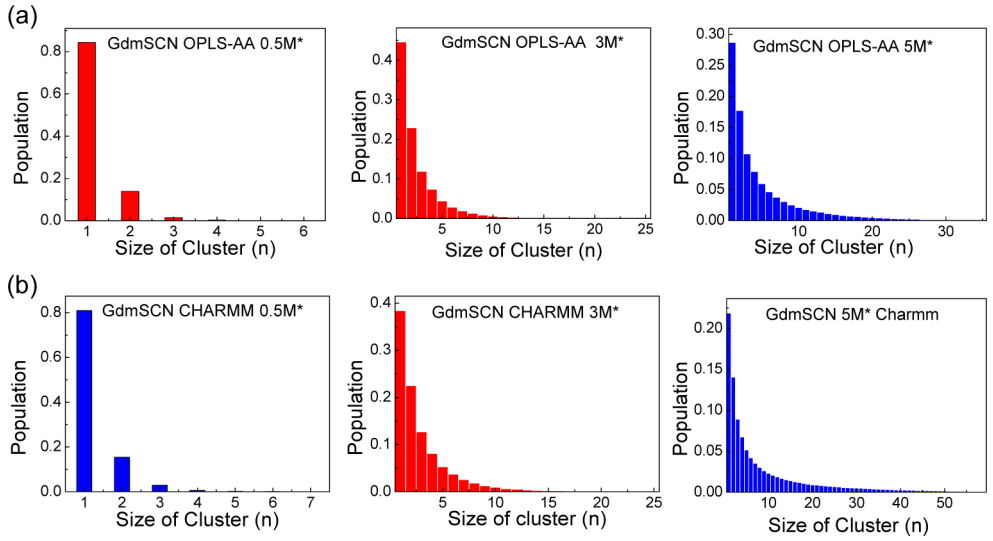

Figure 3. Population distributions of ion species from calculations with (a) the OPLS-AA force field and (b) the CHARMM force field.

3. RESULTS AND DISCUSSION

3.1. Molecular Dynamics Simulations Suggest the Existence of Ion Clustering even in the GdmSCN Solution with a Concentration (0.5 M) Close to Physiological Conditions. We first calculate the ion spatial distributions generated by two different force fields. The calculated radial distribution functions (RDFs) of the N-(SCN^-)−H(Gdm^+) and S(SCN^-)−H(Gdm^+) pairs of 0.5, 3, and 5 M* concentrations are presented in Figure 1. As demonstrated in Figure 1a, calculated by the OPLS-AA force field, the first minimum in the radial distribution function $g_{N-H}(r)$ (between N of SCN^- and H of Gdm^+) is 2.56 Å for 0.5 M*, 2.58 Å for 3 M*, and 2.74 Å for 5 M*, respectively. For the $g_{S-H}(r)$ (between S of SCN^- and H of Gdm^+), the values becomes 2.72, 2.56, and 2.78 Å. Furthermore, in the RDFs calculated by the CHARMM force field, presented in Figure 1b, the first minimum in $g_{N-H}(r)$ is 2.54 Å for 0.5 M*, 2.60 Å for 3 M*, and 2.60 Å for 5 M*. They are 2.84, 2.82, and 2.84 Å in $g_{S-H}(r)$. These minima will be used later for ion cluster calculations.

We then compare the simulation results with the published experimental neutron scattering data[16] through the function $G^{Y}_{H}(r)$, which is composed of four radial distribution functions, $g_{HWOW}(r)$, $g_{HN}(r)$, $g_{HC}(r)$, and $g_{HS}(r)$.[16] The function $G^{Y}_{H}(r)$ calculated with OPLS-AA and CHARMM force field (3 M*) in this work, MD results from Mason's work, and the experimental results are presented in Figure 2a. We can clearly find that there is a shoulder at 1.68 Å in the experimental result. In our simulations, this peak appears at 1.78 Å calculated with the OPLS-AA force field and 1.84 Å calculated with the CHARMM force field. However, the simulation result calculated by Mason et al. does not produce such a peak. Other features along the *x*-axis also show that our calculation results with OPLS-AA and CHARMM force fields agree better with the neutron diffraction with isotopic substitution (NDIS) experiments than simulations in literature.[16] Similar to $G^{Y}_{H}(r)$, the radial distribution function of all H atoms in the system, $g_{HH}(r)$, from all theoretical studies and experiment results are displayed in Figure 2b. Although simulation results based on the OPLS-AA force field do not accurately describe the experimental results at 1.5 Å compared with the other one, all of them accurately reveal the position of the shoulder in experimental results at 1.75 Å. Again, the calculations of all force fields in our study reproduce the NDIS experimental results very well. The radial distribution functions that contains pairwise correlations between all heavy atoms other than hydrogen, $G^{Y}_{Y}(r)$, are displayed in Figure 2c for both our simulation results and the result from literature. Our simulation results show some small shifts in both the peaks and troughs in the radial axis compared with experimental observations. These shifts also appear in the previous MD study. In summary, our calculations reproduce the neutron scattering results very well. The consistency between calculations and experiments can be a good indication that our calculations have captured some major structural properties of the solutions.

As discussed in the Introduction, the neutron scattering results cannot provide information about ion pairing and clustering in the solutions, but MD simulations can reveal some insights. Based on the first minimum in each radial distribution

DOI: 10.1021/acs.jpcb.5b04530
J. Phys. Chem. B 2015, 119, 9893−9904

function as demonstrated in Figure 1, the cluster distributions in the solutions are plotted in Figure 3 and listed in Table 1.

Table 1. Ratio of Clusters in Different Definitions for Each Concentration

	concentration	size ≥ 2 (%)	size ≥ 3 (%)	size ≥ 10 (%)	size ≥ 15 (%)
OPLS-AA	0.5 M* (16)	15.685	1.774	0	0
	3 M* (96)	55.397	32.458	1.775	0.222
	5 M* (158)	71.309	53.557	14.920	7.039
CHARMM	0.5 M* (16)	19.019	3.61	0	0
	3 M* (96)	62.641	41.361	5.152	1.409
	5 M* (158)	78.107	64.039	29.875	20.487

The percentage of ions forming clusters with at least three ions is 1.774% in the 0.5 M* solution, 32.458% in the 3 M* solution, and 53.557% in the 5 M* solution from calculations with the OPLS-AA force field model. Calculations with the CHARMM force field yield larger ion clustering ratios. The percentage increases to 3.61% for the 0.5 M* solution, 41.361% for the 3 M* solution, and 64.039% for the 5 M* solution.

To check how large an ion cluster can form in each solution, we analyze the size probability of the largest cluster in each frame of the trajectory generated from the calculations. The results are plotted in Figure 4. In the 0.5 M* solution, GdmSCN tends to form ion pairs, with a small amount of small ion clusters in the dilute solution. In the 3 M* solution, the most probable largest clusters contain about 5−8 ions in calculations based on the OPLS-AA force field model, and 9−19 ions form in the 5 M* solution. In calculations with the CHARMM force field, GdmSCN tends to form ion clusters with 6−10 ions for the 3 M* solution and clusters with 12−32 ions for the 5 M* solution. The calculated results suggest that no large clusters (greater than tens of nanometers) form in the solutions.

In summary, calculations with the two different force fields show that substantial amounts of ion pairs and clusters form in all three solutions of different concentrations. Larger ion associations are observed in the calculations with the CHARMM force field.

3.2. Gdm^+ Competing with H_2O To Bind to SCN^-. The calculated concentrations of ion clusters in the GdmSCN aqueous solutions are similar to those experimentally determined in the KSCN and NH_4SCN solutions.[23−25,30] However, the nonresonant vibrational energy transfer methods[23,24] previously developed to determine the ion clustering ratios and the direct cation/anion binding cannot be applied to the studies of GdmSCN aqueous solutions because of the lack of isotope labeled GdmSCN species, for example, $GdmS^{13}C^{15}N$, and the bridge energy transfer mechanism (details are provided in Supporting Information). In this work, instead, we use the vibrational excitation lifetime and resonant vibrational energy transfer methods to investigate the ion pairing and clustering in the GdmSCN aqueous solutions revealed by the calculations.

To investigate whether ions form pairs or clusters in the GdmSCN aqueous solutions, we first measured the concentration-dependent vibrational lifetime of the CN stretch first excited state of the anion SCN^- in the solutions. As displayed in Figure 5A, the CN stretch vibrational excitation decays very fast in the dilute (0.05 M) H_2O solution, with a relaxation time constant 2.5 ps. At such a low concentration, the majority of the SCN^- anions are surrounded by H_2O molecules. The fast vibrational relaxation of the CN excitation is mainly caused by the quasi-resonant energy transfer from the CN stretch (2066 cm^{-1}) to the combination band of H_2O at about 2000−2100 cm^{-1}.[24] With the increase of concentration, the relaxation gradually slows. At 3 M, the relaxation time is 3.3 ps. In the saturated solution, it is 3.9 ps. In the melt of GdmSCN at 130 °C, the relaxation is even slower, with a time constant of 10.9 ps. One very likely reason for the observation is that in a more concentrated solution, one SCN^- anion is surrounded by fewer H_2O molecules but more cations or even anions. In other words, more ion pairs and clusters form in a more concentrated solution, and therefore the chance for the CN vibrational energy to transfer to H_2O is smaller and that to the cation is larger. Because the transfer from SCN to H_2O (2.5 ps) is

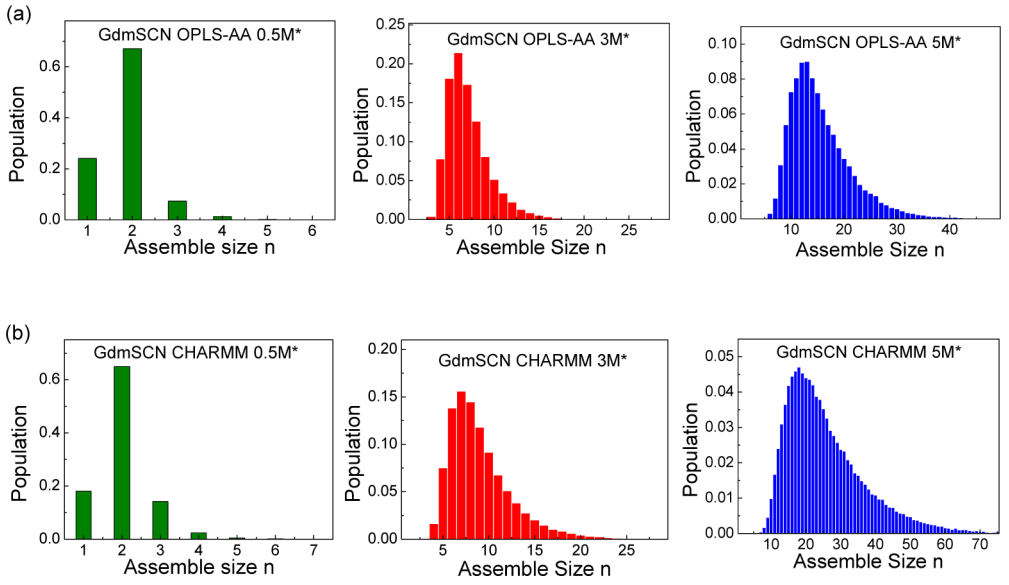

Figure 4. Size probability of the largest cluster in each frame of the trajectory generated from the calculations with (a) the OPLS-AA force field and (b) the CHARMM force field.

DOI: 10.1021/acs.jpcb.5b04530
J. Phys. Chem. B 2015, 119, 9893−9904

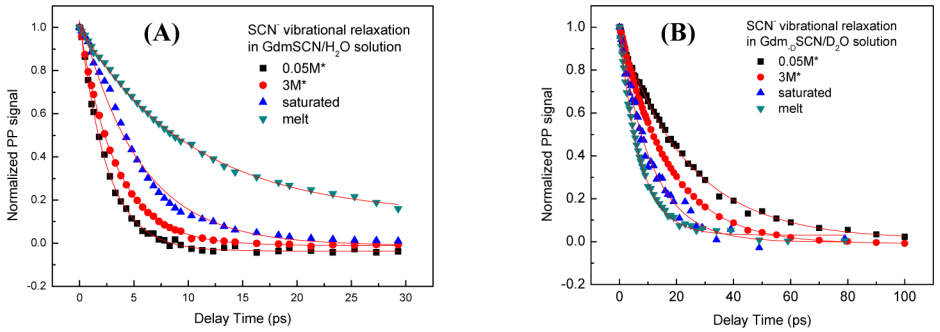

Figure 5. Vibrational relaxations of the CN stretch first excited state of SCN^- in (A) the $GdmSCN/H_2O$ solutions (23 °C) and melt at 130 °C and (B) the $Gdm_{-D}SCN/D_2O$ solutions (23 °C) and melt at 130 °C. In the two solutions, the concentration-dependent vibrational relaxation lifetimes are opposite. Gdm_{-D}^+ is the deuterated Gdm^+ prepared in methanol-OD.

Table 2. Vibrational Relaxation Time of CN Stretch of SCN^- in the First Excited State in $GdmSCN/H_2O$ Solutions and $Gdm_{-D}SCN/D_2O$ Solutions with Different Concentrations

	0.05 M* (23 °C)	0.5 M* (23 °C)	3 M* (23 °C)	5 M* (23 °C)	saturated (23 °C)	saturated (130 °C)	melt[a] (130 °C)
$GdmSCN/H_2O$ (ps)	2.5 ± 0.1	2.7 ± 0.1	3.3 ± 0.1	3.8 ± 0.1	3.9 ± 0.1	4.3 ± 0.1	10.9 ± 0.2
$Gdm_{-D}SCN^b/D_2O$ (ps)	23.7 ± 0.3	22.5 ± 0.2	17.2 ± 0.4	13.2 ± 0.2	12.5 ± 0.2	11.0 ± 0.6	7.0 ± 0.1

[a]There is no water. [b]The sample is deuterated.

significantly faster than to the cation (10.9 ps; the CN intramolecular relaxation is slower than 20 ps, as displayed in Figure 5B), forming more ion pairs or clusters slows down the CN vibrational relaxation. This explanation is further confirmed by the concentration-dependent CN vibrational relaxation experiments in the $Gdm_{-D}SCN/D_2O$ solutions. As displayed in Figure 5B, in a very dilute D_2O solution (0.05 M), the CN vibrational relaxation is very slow, with a time constant 23.7 ps. This result is very different from the H_2O solution of the same concentration where the CN vibrational relaxation is almost 10 times faster. This is because in the D_2O solution, no combination band at 2000−2100 cm^{-1} exists and the energy transfer from CN to D_2O must go through a much slower nonresonant transfer process.[24] In the D_2O solutions, with the concentration increase, the CN vibrational relaxation becomes faster. At 3 M, it is 17.2 ps. In the saturated solution, it is 12.5 ps, and in the melt of $Gdm_{-D}SCN$ (130 °C), it is 7.0 ps. The trend is opposite to that in the H_2O solutions. This, again, can be fully explained by ion pairing and clustering. In a very dilute D_2O solution, the CN vibrational energy can only relax intramolecularly and transfer to D_2O. In a more concentrated solution, more ion pairs and clusters form, and the CN energy can transfer more to the cation Gdm_{-D}^+ and less to D_2O. Because the transfer to the cation (7.0 ps) is faster than that to D_2O (>23.7 ps), more ion pairing and clustering results in a faster CN vibrational relaxation. All the relaxation time constants in both H_2O and D_2O solutions are listed in Table 2.

The concentration-dependent vibrational relaxation times are then analyzed with a simple model to estimate the ratios of ion pairs and clusters in the solutions. The model is based on this simple physical picture: in the solutions, the CN stretch relaxation rate constant of the SCN^- anion, k_{CN}, is the sum from three contributions, the energy transfer to water, $k_{CN\rightarrow water}$, the energy transfer to the cation (Gdm^+ or Gdm_{-D}^+), $k_{CN\rightarrow cation}$, and intramolecular relaxation ($1/k$ = 30 ps[24]). In a very dilute solution, k_{CN} is mainly contributed from the energy transfer to water and the intramolecular relaxation because very few ion pairs or clusters exist. In the melt, k_{CN} is contributed from the energy transfer to the cation and the intramolecular relaxation. In the solutions between the two extremes, we assume $1 - x$ of SCN^- anions bind to water, and the CN energy transfers to water molecules with an energy transfer rate constant $(1 - x)k_{CN\rightarrow water}$. Meanwhile, the rest, x, of the SCN^- anions bind to the cation, and then the CN energy transfers to the cation with an energy transfer rate constant $xk_{CN\rightarrow cation}$. k_{CN}, $k_{CN\rightarrow water}$, and $k_{CN\rightarrow Gdm+}$ can be estimated from the experimental relaxation times. Therefore, the percentage of ion pairing x of the total anions can be deduced from experimental results based on the model. The model is described in the following scheme:

$$k_{CN} - 1/30 = (1 - x)(k_{CN\rightarrow water}) + x(k_{CN\rightarrow cation}) \quad (2)$$

where 30 ps is the intramolecular relaxation lifetime of the CN stretch of SCN^- in water, estimated from both H_2O and D_2O solutions.[24] For the 0.05 M $GdmSCN/H_2O$ solution, from the experimental data we can deduce that $k_{CN\rightarrow H_2O} = 1/2.5 - 1/30 = 1/2.7$ ps^{-1}. For the melt GdmSCN, $k_{CN\rightarrow cation} = 1/10.9 - 1/30 = 1/17.0$ ps^{-1}. For the 3 M $GdmSCN/H_2O$ solution, the experimentally determined $1/k_{CN}$ = 3.3 ps. Based on the parameters and eq 2, the ion pairing percentage in the 3 M $GdmSCN/H_2O$ solution x = 32%. Similarly, we can obtain x = 12%, 46%, and 48% in the 0.5 M, 5 M, and saturated $GdmSCN/H_2O$ solutions, respectively.

The kinetic model eq 2 can be double-checked by data in $Gdm_{-D}SCN/D_2O$ solutions and melt. In the 0.05 M $Gdm_{-D}SCN/D_2O$ solution, from the experimental data, we can deduce that $k_{CN\rightarrow D_2O} = 1/23.7 - 1/30 = 1/113$ ps^{-1}. Based on the relaxation time (7.0 ps) in the melt of $Gdm_{-D}SCN/D_2O$ and eq 2 by assuming the intramolecular relaxation of SCN^- is 30 ps, we can deduce $1/k_{CN\rightarrow cation\text{-}D}$ = 9.1 ps. Using these parameters, we can obtain x = 2.5%, 16%, 34%, and 38% for the 0.5 M, 3 M, 5 M, and saturated $Gdm_{-D}SCN/D_2O$ solutions, respectively.

Combining the results from both $GdmSCN/H_2O$ and $Gdm_{-D}SCN/D_2O$ solutions, we determined the percentage of ion pairing to be 7.3% ± 4.8%, 24% ± 8%, 40% ± 6%, and 43% ± 5% for the 0.5 M, 3 M, 5 M, and saturated solutions, respectively. The relatively large uncertainties of the results

DOI: 10.1021/acs.jpcb.5b04530
J. Phys. Chem. B 2015, 119, 9893−9904

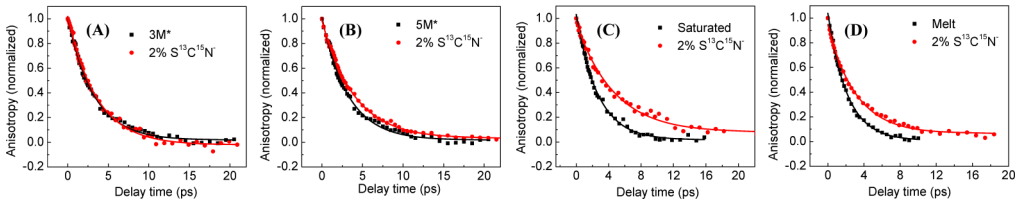

Figure 6. Waiting time dependent anisotropy values of the nitrile stretch vibrational excitation signals in aqueous $Gdm_{-D}SCN/D_2O$ solutions with and without 2% $S^{13}C^{15}N^-$ at concentration (A) 3 M*, (B) 5 M*, and (C) saturated and (D) the melt at 130 °C. Dots are experimental results, and curves are single exponential fits. The black data are from the CN stretch of SCN^- in solutions of which all anions are SCN^-. The anisotropy decays of the black data are contributed from both resonant vibrational energy transfers among SCN^- and the rotation of the anion. The red data are from the $^{13}C^{15}N$ stretch of $S^{13}C^{15}N^-$ in solutions of which the anions contains 2% $S^{13}C^{15}N^-$. The anisotropy decays of the red data are only contributed from the rotation of the anion.

Table 3. Anisotropy Decay Time of SCN^- in $Gdm_{-D}SCN/D_2O$ Solutions and $S^{13}C^{15}N^-$ in $Gdm_{-D}SCN/D_2O$ Solutions with 2% $KS^{13}C^{15}N$

$Gdm_{-D}SCN$[a]/D2O	0.05 M* (23 °C)	0.5 M* (23 °C)	3 M* (23 °C)	5 M* (23 °C)	saturated (23 °C)	melt[b] (130 °C)
anisotropy, τ (ps)	3.0 ± 0.1	3.5 ± 0.1	3.2 ± 0.1	3.1 ± 0.1	2.6 ± 0.1	2.1 ± 0.1
anisotropy, τ_{or} (ps)		3.6 ± 0.1	3.6 ± 0.1	3.9 ± 0.1	4.5 ± 0.1	3.0 ± 0.1

[a]The sample is deuterated. [b]There is no water.

mainly stem from the fact that the exact energy transfer rate constant from the CN stretch to the cation is not known. In the calculations, we used the melt relaxation times at 130 °C to estimate the energy transfer rate constant from the CN stretch to the cation at 23 °C without considering the temperature effect. This can introduce some considerable uncertainties into the results. Compared with the MD simulation results listed in Table 1, the experimental ion pairing percentages are about 100% smaller. There are two possible reasons. One is that in our model, the water/cation exchange, which occurs at the time scale of a few to tens of picoseconds (according to MD simulations), is not considered. The exchange may result in such a consequence: even if all SCN^- anions form ion pairs and clusters, they still have chances to transfer energy to water, and therefore the lifetime of the CN stretch in the solution with 100% ion pairing and clustering can be very different from those in the melt where no water/cation exchange exists. In other words, omitting cation/water exchange underestimates the percentage of ion pairing and clustering. In addition, even if all anions form ion pairs, they still have chances to directly interact with water molecules. Using vibrational lifetimes in the melt does not consider this factor, resulting in the underestimation of the ratio of ion pairing. Therefore, the experimentally estimated ion pairing ratios are only the low limits. The other possible reason for the difference is that the criteria of defining ion pairing are different. In the MD simulations, ion pairs are defined by the first minimum in the radial distribution function. In the experiments, the ion pairs are defined as those that can cause effective vibrational energy transfer between the cation and anion. There is another possible reason that can cause the large difference between the two results. Single exponentials are assumed for the lifetimes of both anion species. This is based on the assumption that the anion chemical exchange is very slow. According to MD simulations, it takes tens of picoseconds for the water and cation bound anions to exchange. This time scale is slower but not much slower than the lifetimes, and therefore the single exponential assumption can induce some uncertainties (<20%). Nonetheless, both simulations and experiments strongly suggest that substantial amounts of ion pairs form in the medium and concentrated solutions.

3.3. SCN^- Anions Forming Clusters with Average Distance about 5.6 Å (5.4 Å) in 3 M (5 M) $Gdm_{-D}SCN/D_2O$ Solution. The concentration-dependent vibrational lifetimes presented above suggest ion pairing in the solutions. However, ion clustering cannot be inferred from the data. To address this issue, we measured the resonant vibrational energy transfers among the anions. The rationale behind the method is that the vibrational energy transfer between two ions is very sensitive to their distance, approximately inversely proportional to the sixth power of the distance.[25] If two anions are solvated by water and therefore well separated from each other, the energy transfer between them will be very slow. If ions form clusters and anions are close to each other, the energy transfer between two anions will be very fast.

Figure 6 displays the waiting time dependent anisotropy values of the nitrile stretch vibrational excitation signals in the aqueous $Gdm_{-D}SCN/D_2O$solutions with and without 2% $S^{13}C^{15}N^-$ at different concentrations. Dots are experimental results, and curves are single exponential fits. The black data are from the CN stretch of SCN^- in solutions of which all anions are SCN^-. The anisotropy decays of the black data are contributed from both resonant vibrational energy transfers among SCN^- and the rotation of the anion. The red data are from the $^{13}C^{15}N$ stretch of $S^{13}C^{15}N^-$ in solutions that contains 2% $S^{13}C^{15}N^-$. The isotope label in $S^{13}C^{15}N^-$ shifts the nitrile stretch frequency by 75 cm^{-1} from that of SCN^-, resulting in the resonant energy transfer among $S^{13}C^{15}N^-$ 50 times slower than that among SCN^-.[26]Therefore, the anisotropy decays of the red data are dominantly contributed from the rotation of the anion.[26] As displayed in Figure 6, the black and red data decay almost at the same rate in the 3 M* solution (Figure 6A). The black data decays slightly faster than the red data in the 5 M* solution (Figure 6B). In the saturated solution (Figure 6C) and the melt (Figure 6D), the black data decays obviously much faster than the red data. The results clearly demonstrate that resonant vibrational energy has transferred among the anions in the concentrated solutions and the melt.

The anisotropy decays in Figure 6 can all be fitted with single exponential decays. The decay constants from the fits are listed in Table 3. In the 3 M* solution, the total anisotropy time constant is 3.2 ps and the rotational time constant is 3.6 ps. The

DOI: 10.1021/acs.jpcb.5b04530
J. Phys. Chem. B 2015, 119, 9893−9904

time constant contributed by energy transfer is therefore 29 ps (1/(1/3.2 − 1/3.6)). In the 5 M* solution, the total anisotropy time constant is 3.1 ps and the rotational time constant is 3.9 ps. The time constant contributed by energy transfer is 15 ps. In the saturated solution, the total anisotropy time constant is 2.6 ps and the rotational time constant is 4.5 ps. The time constant contributed by energy transfer is 6.2 ps. In the melt at 130 °C, the total anisotropy time constant is 2.1 ps and the rotational time constant is 3.0 ps. The time constant contributed by energy transfer is 7.0 ps. It is very interesting that the resonant energy transfer (6.2 ps) in the saturated solution (23 °C) is slightly faster than that (7.0 ps) in the melt at 130 °C. According to our previous studies,[27] resonant energy transfers between two anions in aqueous solutions are faster at a lower temperature. Estimated from the previous studies, the resonant energy transfer time in the assumed melt at 23 °C would be 10−15% faster than that at 130 °C. In other words, the resonant energy transfer rates in the saturated solution and in the melt at the same temperature would be almost identical. Because the transition dipole moments of the nitrile stretch in the saturated solution and the melt are similar, the experimental results suggest that most of the anions form clusters in the saturated solution and the distance between two anions in the saturated solution is similar to that in the melt. This is consistent with the results of the saturated KSCN saturated solution in our previous studies.[25,27] The result also confirms that the ion pairing ratio (<50%) in the saturated solution estimated from the vibrational lifetimes in section 3.2 does underestimate the pairing and clustering ratio.

To extract some quantitative information about the distance between anions in the solutions, we use an approximate model to analyze the anisotropy data.

The experimental pump/probe data for the parallel and perpendicular configurations can be expressed as[46−49]

$$P_{\parallel}(t) = \frac{1}{3}[1 + 2R(t)]P(t) \tag{3}$$

$$P_{\perp}(t) = \frac{1}{3}[1 - R(t)]P(t) \tag{4}$$

where $P(t) = P_{\parallel}(t) + 2P_{\perp}(t)$ describes the excited-state population relaxation. $R(t)$ is the instantaneous anisotropy, which is defined as

$$R(t) = \frac{P_{\parallel}(t) - P_{\perp}(t)}{P_{\parallel}(t) + 2P_{\perp}(t)} \tag{5}$$

In the solutions, as suggested by calculations and experiments, some ions form clusters. The anions in the clusters are close to each other and hence can transfer energy efficiently. Other anions are solvated by water molecules and well separated and less able to transfer energy. Clustered and solvated anions are not frequency resolvable. The energy transfer rate for the separated anions is assumed to be negligibly small because of the relatively long distance between them. In other words, the isolated anions cannot transfer vibrational energy with other isolated anions or with the clustered anions.

As a result, the systems contain two sets of anions that reside in different microenvironments. One is for isolated anions, which are only surrounded by water, and the other is for clustered anions. The anisotropy of the clustered anion, $R_c(t)$, and that of the solvated anion, $R_i(t)$, are defined as[49,50]

$$R_c(t) = \frac{P^c_{\parallel}(t) - P^c_{\perp}(t)}{P^c_{\parallel}(t) + 2P^c_{\perp}(t)} \tag{6}$$

$$R_i(t) = \frac{P^i_{\parallel}(t) - P^i_{\perp}(t)}{P^i_{\parallel}(t) + 2P^i_{\perp}(t)} \tag{7}$$

Where $P^c_{\parallel}(t)$ ($P^i_{\parallel}(t)$) and $P^c_{\perp}(t)$ ($P^i_{\perp}(t)$) are the signal intensities for the clustered anions (isolated anions) with the detection beam parallel and perpendicular to the excitation beam, respectively, at a waiting time t.

$P_{\parallel}(t)$ and $P_{\perp}(t)$ are the sum of all individual components:[49]

$$P_{\parallel}(t) = P^c_{\parallel}(t) + P^i_{\parallel}(t) = \frac{1}{3}[1 + 2R_c(t)]P_c(t) + \frac{1}{3}[1 + 2R_i(t)]P_i(t) \tag{8}$$

$$P_{\perp}(t) = P^c_{\perp}(t) + P^i_{\perp}(t) = \frac{1}{3}[1 - R_c(t)]P_c(t) + \frac{1}{3}[1 - R_i(t)]P_i(t) \tag{9}$$

where $P_c(t)$and $P_i(t)$ describe the excited-state population relaxation of clustered isolated anions with the excited-state lifetime T_c and T_i (23.7 ps, which can be obtained from 0.05 M* $Gdm_{-D}SCN/D_2O$ solution in Table 2), respectively.

According to eq 3, eq 4, eq 8, and eq 9, the sum of the excited-state population relaxation of clustered SCN^- anions and isolated SCN^- anions can be expressed as

$$P(t) = P_c(t) + P_i(t) \tag{10}$$

Hence

$$e^{-t/T} = x\, e^{-t/T_c} + (1 - x)\, e^{-t/T_i} \tag{11}$$

where T is the average excited-state lifetime of both clustered SCN^- anions and isolated SCN^- anions and is determined in Table 2 and x is the percentage of ion cluster. Our previous experiments suggest that the anion/cation ratio in an ion cluster is close to 1/1.[25] Therefore, we simply assume that the cation/anion association ratio obtained in section 3.2 can be approximated as the percentage of ion cluster (x). Then x is determined to be 7.3% (0.5 M*), 24% (3 M*), and 40% (5 M*).

Because there is only one unknown parameter, we can use eq 11 to fit experimental data in Figure 4b. As a result, T_c is determined to be 8.3 ps (3 M*) and 6.8 ps (5 M*) (details are provided in Supporting Information).

According to eq 8 and eq 9, we obtain

$$\begin{aligned} R(t) &= \frac{P_{\parallel}(t) - P_{\perp}(t)}{P_{\parallel}(t) + 2P_{\perp}(t)} \\ &= \frac{(P^c_{\parallel}(t) + P^i_{\parallel}(t)) - (P^c_{\perp}(t) + P^i_{\perp}(t))}{(P^c_{\parallel}(t) + 2P^c_{\perp}(t)) + (P^i_{\parallel}(t) + 2P^i_{\perp}(t))} \\ &= \frac{P^c_{\parallel}(t) - P^c_{\perp}(t)}{P_c(t)}\frac{P_c(t)}{P(t)} + \frac{P^i_{\parallel}(t) - P^i_{\perp}(t)}{P_i(t)}\frac{P_i(t)}{P(t)} \\ &= f_c R_c(t) + f_i R_i(t) \end{aligned} \tag{12}$$

where f_c (f_i) represents the fraction of clustered SCN^- anions (isolated SCN^- anions) with a fixed anisotropy $R_c(t)$ ($R_i(t)$) contributing to the total signal intensity.

On the basis of eq 11, we can further obtain

DOI: 10.1021/acs.jpcb.5b04530
J. Phys. Chem. B 2015, 119, 9893−9904

$$f_c = \frac{P_c(t)}{P(t)} = x \exp\left[t\left(-\frac{1}{T_c} + \frac{1}{T}\right)\right] \quad (13)$$

$$f_i = \frac{P_i(t)}{P(t)} = (1-x) \exp\left[t\left(-\frac{1}{T_i} + \frac{1}{T}\right)\right] \quad (14)$$

where T is the average excited-state lifetime of both clustered SCN^- anions and isolated SCN^- anions and x is the percentage of ion cluster. f_c [f_i] equals $x\, e^{t(-(1/8.3)+(1/17.2))} = x\, e^{(-t/16)}$ [$(1-x)\, e^{t(-(1/23.7)+(1/17.2))} = (1-x)\, e^{(t/62.7)}$] and $x\, e^{t(-(1/6.8)+(1/13.2))} = x\, e^{(-t/14)}$ [$(1-x)\, e^{t(-(1/23.7)+(1/13.2))} = (1-x)\, e^{(t/30)}$] in 3 M* and 5 M* $Gdm_{-D}SCN/D_2O$ solutions, respectively.

From the above derivation, we know that f_c (f_i) is different from the molar fraction of the clustered SCN^- anions (isolated SCN^- anions) of molecules in the sample.

As discussed above, in our experiment,[31] there are two contributions to the signal anisotropy decay. One is the molecular rotation, and the other is the resonant energy transfer from one anion to another randomly oriented anion. In a $Gdm_{-D}SCN/D_2O$ solution with 2% $S^{13}C^{15}N^-$, the anisotropy decay of the $S^{13}C^{15}N^-$ signals of clustered and isolated SCN^- anions are mostly caused by the molecular rotation because $S^{13}C^{15}N^-$ anions are too far away to effectively exchange energy. Therefore, based on eq 12, eq 13, eq 14, and the above calculated values, the total anisotropy of 3 M* $Gdm_{-D}SCN/D_2O$ solution can be expressed as

$$\begin{aligned} R(t) &= x \exp\left[\frac{-t}{16}\right] R_c(t) + (1-x) \exp\left[\frac{t}{62.7}\right] R_i(t) \\ &= x \exp\left[-t\left(\frac{1}{16} + \frac{1}{\tau^c_{or}}\right)\right] + (1-x) \\ &\quad \exp\left[-t\left(-\frac{1}{62.7} + \frac{1}{\tau^i_{or}}\right)\right] \\ &= x \exp\left[-t\left(\frac{1}{16} + \frac{1}{\tau^c_{or}}\right)\right] + (1-x) \exp\left[\frac{-t}{3.2}\right] \end{aligned} \quad (15)$$

and the total anisotropy of 5M* $Gdm_{-D}SCN/D_2O$ solution can be expressed as

$$\begin{aligned} R(t) &= x \exp\left[\frac{-t}{14}\right] R_c(t) + (1-x) \exp\left[\frac{t}{30}\right] R_i(t) \\ &= x \exp\left[-t\left(\frac{1}{14} + \frac{1}{\tau^c_{or}}\right)\right] + (1-x) \\ &\quad \exp\left[-t\left(-\frac{1}{30} + \frac{1}{\tau^i_{or}}\right)\right] \\ &= x \exp\left[-t\left(\frac{1}{14} + \frac{1}{\tau^c_{or}}\right)\right] + (1-x) \exp\left[\frac{-t}{3.3}\right] \end{aligned} \quad (16)$$

where τ_{or} is the total anisotropy decay time constant of the solution with 2% $S^{13}C^{15}N^-$, τ^c_{or} (τ^i_{or}) is molecular rotational time constant of the clustered (isolated) $S^{13}C^{15}N^-$, the very small influence caused by the mass differences among the C and N isotopes is ignored, and τ^i_{or} (3.0 ps) is obtained from the anisotropy decay time constant in the 0.05 M solution with 2% $KS^{13}C^{15}N$ in Table 3.

Therefore, we can use eq 15 and eq 16 to fit experimental data in Figure 6. As a result, τ^c_{or} is determined to be 8.4 ps (3 M*), and 8.3 ps (5 M*), respectively (details are provided in Supporting Information).

In a solution with 100% $Gdm_{-D}SCN$, the anisotropy decay of the SCN^- signal of clustered anions is from both molecular rotations and resonant energy transfers with a time constant τ^c, while the anisotropy decay of the SCN^- signal of isolated anions is only from molecular rotations with a time constant τ^i_{or}. Therefore, similarly, the total anisotropy of 3 M* $Gdm_{-D}SCN/D_2O$ solution can be expressed as

$$\begin{aligned} R(t) &= x \exp\left[\frac{-t}{16}\right] R_c(t) + (1-x) \exp\left[\frac{t}{62.7}\right] R_i(t) \\ &= x \exp\left[-t\left(\frac{1}{16} + \frac{1}{\tau^c}\right)\right] + (1-x) \\ &\quad \exp\left[-t\left(-\frac{1}{62.7} + \frac{1}{\tau^i_{or}}\right)\right] \\ &= x \exp\left[-t\left(\frac{1}{16} + \frac{1}{\tau^c}\right)\right] + (1-x) \exp\left[\frac{-t}{3.2}\right] \end{aligned} \quad (17)$$

and the total anisotropy of 5M* $Gdm_{-D}SCN/D_2O$ solution can be expressed as

$$\begin{aligned} R(t) &= x \exp\left[\frac{-t}{14}\right] R_c(t) + (1-x) \exp\left[\frac{t}{30}\right] R_i(t) \\ &= x \exp\left[-t\left(\frac{1}{14} + \frac{1}{\tau^c}\right)\right] + (1-x) \\ &\quad \exp\left[-t\left(-\frac{1}{30} + \frac{1}{\tau^i_{or}}\right)\right] \\ &= x \exp\left[-t\left(\frac{1}{14} + \frac{1}{\tau^c}\right)\right] + (1-x) \exp\left[\frac{-t}{3.3}\right] \end{aligned} \quad (18)$$

Therefore, we can use eq 17 and eq 18 to fit experimental data in Figure 6. As a result, τ^c is determined to be 4.2 ps (3 M*), and 3.3 ps (5 M*) (details are provided in Supporting Information).

Based on the above fitted values, the resonant energy transfer time constant τ^c_e ($=1/(1/\tau^c - 1/\tau^i_{or})$) of clustered anions is determined to be 8.4 ps (3 M*) and 5.5 ps (5 M*). The faster energy transfer in a more concentrated solution indicates a larger ion cluster, consistent with the MD results and our previous results.[23]

The energy transfer time constants can be converted into the distance between two anions through the energy transfer equation derived from our previous works[25−27]

$$k_{DA} = \frac{2}{1 + e^{-\Delta\omega_{DA}/(RT)}} V_{DA}{}^2 \frac{\tau^{-1}}{(\Delta\omega_{DA})^2 + 4V_{DA}{}^2 + \tau^{-2}} \quad (19)$$

where $\Delta\omega_{DA} = \omega_D - \omega_A$, the difference between the central energy values of D and A, also termed the donor/acceptor (D/A) energy gap (this value is equal to 0 for the resonant energy transfer), τ is the dephasing time of the coherence between the

DOI: 10.1021/acs.jpcb.5b04530
J. Phys. Chem. B 2015, 119, 9893−9904

donor and acceptor, and V_{DA} is the D/A coupling strength, which quantitatively correlated to the donor/acceptor distance (r_{DA}) under the dipole/dipole interaction mechanism by

$$V_{DA}^{\ 2} = \frac{1}{n^4}\frac{\mu_D^{\ 2}\mu_A^{\ 2}}{(4\pi\varepsilon_0)^2}\frac{\kappa^2}{r_{DA}^{\ 6}} \tag{20}$$

where n is the refractive index, μ_D and μ_A are the respective transition dipole moments of the donor and acceptor, ε_0 is the vacuum permittivity, r_{DA} is the distance between the donor and acceptor, and κ is the orientation factor dependent on the relative orientations of the donor/acceptor and the relative time scales of the rotations of the donor/acceptor and the energy transfer.

In the solutions studied here, the distance between two ions is typically larger than the length of a chemical bond (or a vibrational mode), and the vibrational coupling between two modes is typically smaller than the vibrational dephasing line widths of the model.[26,27] As a result, eqs 19 and 20 can be approximated into

$$k_{DA} \propto \left(\frac{1}{r_{DA}}\right)^6 \tag{21}$$

From our previous works,[23,27] we can know that in the 3 M* and 5 M* KSCN/H_2O solutions, anions form clusters with average anion distances about 4.4 and 4.6 Å and resonant energy transfer rate constants are about 1/4.5 ps^{-1} and 1/5 ps^{-1}. Meanwhile, we also find that the number of clusters that are predicted by MD simulations between the KSCN/H_2O solutions and the GdmSCN/H_2O are very similar. As a result, we can roughly assume that the size of clusters in both solutions are the same and compare the two systems to estimate the average anion distances in the GdmSCN solutions based on eq 21. The estimated average anion distances for the clustered anions are 4.9 and 4.7 Å in 3 M* and 5 M* $Gdm_{-D}SCN/D_2O$ solutions, respectively. We notice that if we assume that almost all anions form clusters in the saturated $Gdm_{-D}SCN/D_2O$ solution as that happens in the saturated KSCN aqueous solution, the resonant energy transfer times in both solutions are about 100% different, −6.2 ps for $Gdm_{-D}SCN$ and 3.0 ps[27] for KSCN. The energy transfer rate difference (100%), which is equivalent to the distance difference (12%), is probably because Gdm is a larger cation than K^+. Using the underestimated pairing ratio obtained from the vibrational lifetimes, we calculate the resonant energy transfer time in the saturated $Gdm_{-D}SCN/D_2O$ solution to be 2.7 ps (details are provided in Supporting Information). This energy transfer rate is overestimated for about 100%. Corrected with this factor, the estimated average anion distances for the clustered anions are 5.6 and 5.4 Å in the 3 M* and 5 M* $Gdm_{-D}SCN/D_2O$ solutions, respectively. These values are consistent with the results of MD simulation (details are provided in Supporting Information). They are about 14% larger than those in the KSCN solutions.[27]

In the 3 M and 5 M GdmSCN aqueous solution, if the ions do not form clusters and are well separated by water, the nominal average anion distance estimated from the liquid density, is r_{3M} = 9.0 Å and r_{5M} = 7.9 Å. These two values are significantly larger than 5.6 and 5.4 Å estimated from the resonant energy transfer rates. The comparison strongly suggests that ions form clusters in the solutions.

4. CONCLUDING REMARKS

In this work, MD simulations with two different force fields, vibrational energy relaxation and resonant energy transfer experiments, and neutron scattering data are used to investigate ion pairing and clustering in a series of GdmSCN aqueous solutions. The MD simulations reproduce the major features of neutron scattering experimental data very well. Although no information about ion pairing or clustering can be obtained from the neutron scattering data, MD calculations clearly demonstrate that substantial amounts of ion pairs and small ion clusters do exist in the solutions of concentrations 0.5, 3, and 5 M*. Vibrational relaxation experiments suggest that significant amounts of ion pairs form in the solutions. Experiments measuring the resonant energy transfers among the thiocyanate anions in the solutions suggest that the ions form clusters, and in the clusters the average anion distances are 5.6 and 5.4 Å in the 3 M* and 5 M* $Gdm_{-D}SCN/D_2O$ solutions, respectively. This work demonstrates that ultrafast vibrational energy transfer methods can be very helpful in the studies of ion pairing and ion clustering in strong electrolyte aqueous solutions that are difficult to investigate by neutron scattering. We expect that with the increased availability of ultrafast lasers, the vibrational energy transfer methods can be applied to more systems in different fields.

■ ASSOCIATED CONTENT

Supporting Information

FTIR spectra of GdmSCN/H_2O (3 M) and GdmSCN/D_2O, waiting time dependent 2D IR spectra of the GdmSCN/D_2O (3 M), derivation of pair distribution functions of GdmSCN solution, experimental set-up, cross section and neutron scattering length, mean absolute intensity, final intensity of neutrons, first-order and second-order difference scattering functions, single exponential fitting of vibrational relaxation and anisotropy relaxation, double exponential fitting of vibrational relaxation and anisotropy relaxation, and RDFs of $C(SCN^-)$–$N(SCN^-)$, $C(SCN^-)$–$C(SCN^-)$ and $N(SCN^-)$–$N(SCN^-)$. The Supporting Information is available free of charge on the ACS Publications website at DOI: 10.1021/acs.jpcb.5b04530.

■ AUTHOR INFORMATION

Corresponding Authors

*E-mail: kjyuan@dicp.ac.cn.
*E-mail: wzhuang@dicp.ac.cn.
*E-mail: junrong@rice.edu.

Author Contributions

¶Y.S., T.W., and B.J. have contributed equally.

Notes

The authors declare no competing financial interest.

■ ACKNOWLEDGMENTS

This material is based upon work supported by the AFOSR Award No. FA9550-11-1-0070 and the Welch foundation under Award No.C-1752. J. R. Zheng also thanks the David and Lucile Packard Foundation for a Packard fellowship and the Alfred P. Sloan Foundation for a Sloan fellowship. KJY thanks the support by the National Natural Science Foundation of China (No. 21373213), the Chinese Academy of Sciences, and the Ministry of Science and Technology. WZ thanks the support by the NSFC Grant 21373201, NSFC key Grant 21033008 and Science and Technological Ministry of China Grant 2011YQ09000505. We thank Doctor Ke Lin at USTC

DOI: 10.1021/acs.jpcb.5b04530
J. Phys. Chem. B 2015, 119, 9893−9904

for discussion of the application of Raman spectroscopy in determining ion clustering.

REFERENCES

(1) Gebauer, D.; Volkel, A.; Colfen, H. Stable Prenucleation Calcium Carbonate Clusters. *Science* **2008**, *322*, 1819−1822.

(2) Pouget, E. M.; Bomans, P. H. H.; Goos, J.; Frederik, P. M.; de With, G.; Sommerdijk, N. The Initial Stages of Template-Controlled Caco3 Formation Revealed by Cryo-Tem. *Science* **2009**, *323*, 1455−1458.

(3) Gebauer, D.; Colfen, H. Prenucleation Clusters and Non-Classical Nucleation. *Nano Today* **2011**, *6*, 564−584.

(4) Wallace, A. F.; Hedges, L. O.; Fernandez-Martinez, A.; Raiteri, P.; Gale, J. D.; Waychunas, G. A.; Whitelam, S.; Banfield, J. F.; De Yoreo, J. J. Microscopic Evidence for Liquid-Liquid Separation in Supersaturated Caco3 Solutions. *Science* **2013**, *341*, 885−889.

(5) Demichelis, R.; Raiteri, P.; Gale, J. D.; Quigley, D.; Gebauer, D. Stable Prenucleation Mineral Clusters Are Liquid-Like Ionic Polymers. *Nat. Commun.* **2011**, *2*, 590.

(6) Myerson, A. S.; Trout, B. L. Nucleation from Solution. *Science* **2013**, *341*, 855−856.

(7) DiMasi, E.; Gower, L. B. *Biomineralization Sourcebook: Characterization of Biominerals and Biomimetic Materials*; CRC Press: Boca Raton, FL, 2014.

(8) Soper, A.; Neilson, G.; Enderby, J.; Howe, R. A Neutron Diffraction Study of Hydration Effects in Aqueous Solutions. *J. Phys. C: Solid State Phys.* **1977**, *10*, 1793.

(9) Enderby, J. E.; Neilson, G. W. The Structure of Electrolyte Solutions. *Rep. Prog. Phys.* **1981**, *44*, 593−653.

(10) Neilson, G. W.; Enderby, J. E. The Structure of an Aqueous-Solution of Nickel Chloride. *Proc. R. Soc. London, Ser. A* **1983**, *390*, 353−371.

(11) Neilson, G. W.; Enderby, J. E. The Coordination of Metal Aquaions. *Adv. Inorg. Chem.* **1989**, *34*, 195−218.

(12) Broadbent, R. D.; Neilson, G. W. The Interatomic Structure of Argon in Water. *J. Chem. Phys.* **1994**, *100*, 7543−7547.

(13) Sullivan, D. M.; Neilson, G. W.; Fischer, H. E. Hydrophobic Hydration of Argon at High Temperatures. *J. Chem. Phys.* **2001**, *115*, 339−343.

(14) Barnes, A. C.; Neilson, G. W.; Enderby, J. E. The Structure and Dynamics of Aqueous Solutions Containing Complex Molecules. *J. Mol. Liq.* **1995**, *65/66*, 99−106.

(15) Turner, J. Z.; Soper, A. K.; Finney, J. L. Ionic Versus Apolar Behavior of the Tetramethylammonium Ion in Water. *J. Chem. Phys.* **1995**, *102*, 5438−5443.

(16) Mason, P. E.; Dempsey, C. E.; Neilson, G. W.; Brady, J. W. Nanometer-Scale Ion Aggregates in Aqueous Electrolyte Solutions: Guanidinium Sulfate and Guanidinium Thiocyanate. *J. Phys. Chem. B* **2005**, *109*, 24185−24196.

(17) Georgalis, Y.; Kierzek, A. M.; Saenger, W. Cluster Formation in Aqueous Electrolyte Solutions Observed by Dynamic Light Scattering. *J. Phys. Chem. B* **2000**, *104*, 3405−3406.

(18) Frost, R. L.; James, D. W. Ion-Ion-Solvent Interactions in Solution Part 3.-Aqueous Solutions of Sodium Nitrate. *J. Chem. Soc., Faraday Trans. 1* **1982**, *78*, 3223−3234.

(19) Rusli, I. T.; Schrader, G. L.; Larson, M. A. Raman Spectroscopic Study of Nano3 Solution System - Solute Clustering in Supersaturated Solutions. *J. Cryst. Growth* **1989**, *97*, 345−351.

(20) Cerreta, M. K.; Berglund, K. A. The Structure of Aqueous Solutions of Some Dihydrogen Orthophosphates by Laser Raman Spectroscopy. *J. Cryst. Growth* **1987**, *84*, 577−588.

(21) Wang, C. C.; Lin, K.; Hu, N. Y.; Zhou, X. G.; Liu, S. L. Ion Pairs in Aqueous Magnesium Nitrate Solution by Excess Raman Spectroscopy. *Acta Phys.-Chim. Sin.* **2012**, *28*, 1823−1829.

(22) Bian, H.; Chen, H.; Li, J.; Wen, X.; Zheng, J. Nonresonant and Resonant Mode-Specific Intermolecular Vibrational Energy Transfers in Electrolyte Aqueous Solutions. *J. Phys. Chem. A* **2011**, *115*, 11657−11664.

(23) Bian, H. T.; Wen, X. W.; Li, J. B.; Chen, H. L.; Han, S. Z.; Sun, X. Q.; Song, J. A.; Zhuang, W.; Zheng, J. R. Ion Clustering in Aqueous Solutions Probed with Vibrational Energy Transfer. *Proc. Natl. Acad. Sci. U. S. A.* **2011**, *108*, 4737−4742.

(24) Li, J.; Bian, H.; Chen, H.; Wen, X.; Hoang, B. T.; Zheng, J. Ion Association in Aqueous Solutions Probed through Vibrational Energy Transfers among Cation, Anion, and Water Molecules. *J. Phys. Chem. B* **2013**, *117*, 4274−4283.

(25) Chen, H.; Bian, H.; Li, J.; Wen, X.; Zhang, Q.; Zhuang, W.; Zheng, J. Vibrational Energy Transfer: An Angstrom Molecular Ruler in Studies of Ion Pairing and Clustering in Aqueous Solutions. *J. Phys. Chem. B* **2015**, *119*, 4333−4349.

(26) Chen, H.; Wen, X.; Li, J.; Zheng, J. Molecular Distances Determined with Resonant Vibrational Energy Transfers. *J. Phys. Chem. A* **2014**, *118*, 2463−2469.

(27) Chen, H.; Wen, X.; Guo, X.; Zheng, J. Intermolecular Vibrational Energy Transfers in Liquids and Solids. *Phys. Chem. Chem. Phys.* **2014**, *16*, 13995−14014.

(28) Bian, H.; Li, J.; Wen, X.; Zheng, J. Mode-Specific Intermolecular Vibrational Energy Transfer. I. Phenyl Selenocyanate and Deuterated Chloroform Mixture. *J. Chem. Phys.* **2010**, *132*, 184505.

(29) Bian, H.; Wen, X.; Li, J.; Zheng, J. Mode-Specific Intermolecular Vibrational Energy Transfer. Ii. Deuterated Water and Potassium Selenocyanate Mixture. *J. Chem. Phys.* **2010**, *133*, 034505.

(30) Chen, H. L.; Bian, H. T.; Li, J. B.; Wen, X. W.; Zheng, J. R. Ultrafast Multiple-Mode Multiple-Dimensional Vibrational Spectroscopy. *Int. Rev. Phys. Chem.* **2012**, *31*, 469−565.

(31) Yuan, K.; Bian, H.; Shen, Y.; Jiang, B.; Li, J.; Zhang, Y.; Chen, H.; Zheng, J. Coordination Number of Li^+ in Nonaqueous Electrolyte Solutions Determined by Molecular Rotational Measurements. *J. Phys. Chem. B* **2014**, *118*, 3689−3695.

(32) Hess, B.; Kutzner, C.; van der Spoel, D.; Lindahl, E. Gromacs 4: Algorithms for Highly Efficient, Load-Balanced, and Scalable Molecular Simulation. *J. Chem. Theory Comput.* **2008**, *4*, 435−447.

(33) Jorgensen, W. L.; Maxwell, D. S.; TiradoRives, J. Development and Testing of the Opls All-Atom Force Field on Conformational Energetics and Properties of Organic Liquids. *J. Am. Chem. Soc.* **1996**, *118*, 11225−11236.

(34) Kaminski, G. A.; Friesner, R. A.; Tirado-Rives, J.; Jorgensen, W. L. Evaluation and Reparametrization of the Opls-Aa Force Field for Proteins Via Comparison with Accurate Quantum Chemical Calculations on Peptides. *J. Phys. Chem. B* **2001**, *105*, 6474−6487.

(35) Berendsen, H. J. C.; Grigera, J. R.; Straatsma, T. P. The Missing Term in Effective Pair Potentials. *J. Phys. Chem.* **1987**, *91*, 6269−6271.

(36) Mason, P. E.; Neilson, G. W.; Enderby, J. E.; Saboungi, M. L.; Dempsey, C. E.; MacKerell, A. D.; Brady, J. W. The Structure of Aqueous Guanidinium Chloride Solutions. *J. Am. Chem. Soc.* **2004**, *126*, 11462−11470.

(37) Mackerell, A. D.; Feig, M.; Brooks, C. L. Extending the Treatment of Backbone Energetics in Protein Force Fields: Limitations of Gas-Phase Quantum Mechanics in Reproducing Protein Conformational Distributions in Molecular Dynamics Simulations. *J. Comput. Chem.* **2004**, *25*, 1400−1415.

(38) Vincze, A.; Jedlovszky, P.; Horvai, G. The L/L Interface and Adsorption of Scn^- Anions as Studied by Different Molecular Simulation Techniques. *Anal. Sci./Suppl.* **2002**, *17icas*, i317−i320.

(39) Sansone, R.; Ebner, C.; Probst, M. Quantum Chemical and Molecular Dynamics Study on the Hydration of Cyanide and Thiocyanate Anions. *J. Mol. Liq.* **2000**, *88*, 129−150.

(40) Darden, T.; York, D.; Pedersen, L. Particle Mesh Ewald - an N.Log(N) Method for Ewald Sums in Large Systems. *J. Chem. Phys.* **1993**, *98*, 10089−10092.

(41) Hockney, R. W.; Goel, S. P.; Eastwood, J. W. Quiet High-Resolution Computer Models of a Plasma. *J. Comput. Phys.* **1974**, *14*, 148−158.

(42) Essmann, U.; Perera, L.; Berkowitz, M. L.; Darden, T.; Lee, H.; Pedersen, L. G. A Smooth Particle Mesh Ewald Method. *J. Chem. Phys.* **1995**, *103*, 8577−8593.

DOI: 10.1021/acs.jpcb.5b04530
J. Phys. Chem. B 2015, 119, 9893−9904

(43) Frenkel, D.; Smit, B. *Understanding Molecular Simulation: From Algorithms to Applications*, 2nd ed.; Academic Press: New York, 2001.
(44) Berendsen, H. J. C.; Postma, J. P. M.; Vangunsteren, W. F.; Dinola, A.; Haak, J. R. Molecular-Dynamics with Coupling to an External Bath. *J. Chem. Phys.* **1984**, *81*, 3684−3690.
(45) Zhang, Q.; Xie, W.; Bian, H.; Gao, Y. Q.; Zheng, J.; Zhuang, W. Microscopic Origin of the Deviation from Stokes−Einstein Behavior Observed in Dynamics of the Kscn Aqueous Solutions: A Md Simulation Study. *J. Phys. Chem. B* **2013**, *117*, 2992−3004.
(46) Kinosita, K., Jr; Kawato, S.; Ikegami, A. A Theory of Fluorescence Polarization Decay in Membranes. *Biophys. J.* **1977**, *20*, 289−305.
(47) Tokmakoff, A.; Urdahl, R. S.; Zimdars, D.; Francis, R. S.; Kwok, A. S.; Fayer, M. D. Vibrational Spectral Diffusion and Population-Dynamics in a Glass-Forming Liquid - Variable Bandwidth Picosecond Infrared-Spectroscopy. *J. Chem. Phys.* **1995**, *102*, 3919−3931.
(48) Tan, H. S.; Piletic, I. R.; Fayer, M. D. Polarization Selective Spectroscopy Experiments: Methodology and Pitfalls. *J. Opt. Soc. Am. B* **2005**, *22*, 2009−2017.
(49) Valeur, B.; Berberan-Santos, M. N. *Molecular Fluorescence: Principles and Applications*; Wiley-VCH: Weinheim, Germany, 2012.
(50) Chen, H. L.; Bian, H. T.; Li, J. B.; Wen, X. W.; Zheng, J. R. Relative Intermolecular Orientation Probed Via Molecular Heat Transport. *J. Phys. Chem. A* **2013**, *117*, 6052−6065.

DOI: 10.1021/acs.jpcb.5b04530
J. Phys. Chem. B 2015, 119, 9893−9904